An iterative deconvolution algorithm using combined regularization for low-order corrected astronomical images

Hualin Chen[1,2], Xiangyan Yuan[1], Xiangqun Cui[1]

1. National Astronomical Observatories/Nanjing Institute of Astronomical Optics & Technology, Chinese Academy of Sciences, Nanjing 210042, China
2. Graduate School of the Chinese Academy of Sciences, Beijing 100049

ABSTRACT

An iterative deconvolution algorithm is presented in detail which utilizes regularization to combine maximum-likelihood (ML) estimate of convolution error and several physical constraints to build error function. The physical constraints used in this algorithm include positivity, band-limit information and the information of multiple frames. By minimizing the combined error metric of individual ones, the object can be expected to be recovered from the noisy data. In addition, numerical simulation of Phase Screen distorted by atmospheric turbulence following the Kolmogorov spectrum is also made to generate the PSFs which are used to simulate the degraded images.

Keywords: adaptive optics, iterative deconvolution, maximum-likelihood, physical constraints

1. INTRODUCTION

Besides the inherent defects of the instrument's optics, ground-based images are severely distorted due to the atmospheric turbulence. Without correction, the angular spatial resolution is limited to the ratio wavelength over fried's parameter. In many past years, various techniques have been proposed to overcome this limitation and efficiently reach the diffraction limit of the telescopes. Adaptive optics (AO) is now a proven powerful technology for real-time compensation of space objects, to reduce the degrading effects of the Earth's atmosphere. However, the compensation is never "perfect" and residual wave-front errors remain, which in some cases can lead to significant uncompensated power. This decreases the image contrast making, in some cases, necessary to use some form of image post-processing to remove these effects. In this paper, we use regularization to combine maximum-likelihood (ML) estimate[1] and physical constraint[2, 3, 4, 5, 6]. As previously mentioned, the algorithm can be expected to recover the object.

2. THE DECONVOLUTION PROBLEM

The linear imaging equation can be written as

$$g'(\vec{r}) = f(\vec{r}) * h(\vec{r}) + n(\vec{r}) \tag{1}$$

or in the Fourier domain as

$$G'(\vec{u}) = F(\vec{u})H(\vec{u}) + N(\vec{u}) \tag{2}$$

where $g'(\vec{r})$ is the measurement, $f(\vec{r})$ is the object, $h(\vec{r})$ is the PSF of system, $n(\vec{r})$ represents noise contamination and $*$ denotes convolution. The Fourier transforms are indicated by the corresponding uppercase notation, where $\vec{r}$ and $\vec{u}$ are the spatial index and the spatial frequency index respectively.

Email: hualinchen@niaot.ac.cn

Adaptive Optics Systems, edited by Norbert Hubin, Claire E. Max, Peter L. Wizinowich,
Proc. of SPIE Vol. 7015, 70152F, (2008)
0277-786X/08/$18 · doi: 10.1117/12.787564

The inverse problem to determine f is usually an ill-posed problem in practice. This means that there is no unique and stable solution. But, we can introduce regularization in order to find a unique and stable solution.

3. DECONVOLUTION BY MAXIMUM-LIKELIHOOD (ML) ESTIMATE OF CONVOLUTION ERROR AND SOME PHYSICAL CONSTRAINTS

3.1 ML estimate of convolution Error

The convolution error measures the consistency between the measurements and the estimates, and is defined as

$$E_F = \sum_k \left\| g'_k - \hat{f} * \hat{h}_k \right\|^2 \tag{3}$$

where k is the frame index， the ^ indicates the current estimates of the variables, and $\|\cdot\|$ denotes Frobenius norm. On the other hand, by M-L theory and Tikhonov regularization theory, (3) is equivalent to

$$J = \frac{1}{2}\left(\sum_k \left\| g'_k - \hat{f} * \hat{h}_k \right\|^2\right) + \frac{\gamma}{2}\left\|\hat{f}\right\|^2 \tag{4}$$

where γ is the regular factor. (4) can be transformed as

$$J = \frac{1}{2}\left(\sum_k \left\| G'_k - \hat{F}\hat{H}_k \right\|^2\right) + \frac{\gamma}{2}\left\|\hat{F}\right\|^2 \tag{5}$$

Setting derivate of J respective with $\hat{F}$ equal to zeros, we can get

$$\hat{F} = \frac{\sum_k \hat{H}^* G'_k}{\gamma + \sum_k \left|\hat{H}_k\right|^2} \tag{6}$$

Thus,

$$J = \frac{1}{2}\left(\sum_k \left\| G'_k \right\|^2 - \left\| \frac{\sum_k G'^*_k \hat{H}_k}{\left(\gamma + \sum_k \left|\hat{H}_k\right|^2\right)^{\frac{1}{2}}} \right\|^2\right) \tag{7}$$

Here, using (7) to represent convolution error. So,

$$E_F = \sum_k \left\| G'_k \right\|^2 - \left\| \frac{\sum_k G'^*_k \hat{H}_k}{\left(\gamma + \sum_k \left|\hat{H}_k\right|^2\right)^{\frac{1}{2}}} \right\|^2 \tag{8}$$

3.2 Positive

Due to physical constraints to both the object and PSF, both are positive and are parameterized as square quantities for convenience of programming and error metric minimization, i.e.

$$\hat{f}_i = \phi_i^2 \qquad \text{and} \qquad \hat{h}_{ik} = \varphi_{ik}^2 \tag{9}$$

3.3 Band-Limit Error

The PSF band-limit error is defined as

$$E_{BL} = \sum_k \left\| \Lambda \hat{H}_k \right\|^2 \tag{10}$$

where $\Lambda = \begin{cases} 1 & , \ u > f_c \\ 0 & , \ \text{others} \end{cases}$, and f_c is a appropriate cut-off frequency. This constraint can force high-spatial frequency noise into the PSF estimates.

3.4 Prior PSF Information

Prior PSF information can be used to reduce the PSF parameter space, to better prevent local minimum, and also break the symmetry. We use the form of a mean PSF for multiple PSFs[6] to do this. The mean PSF, denoted by h_{SAA} (this means the shift-and-add (SAA) or peak-stacked mean of the PSFs), can remove the effects of mis-registration from one frame to another. The SAA of the PSF estimates is

$$\left(\hat{h}_i\right)_{SAA} = \frac{1}{K}\sum_k \hat{h}_{k(i-\hat{p}_k)} \tag{11}$$

where $\hat{p}_k$ is the intensity peak location of the kth frame, and K is the number of frame. Then, the SAA image is compared to the SAA image of a reference star (denoted by $(h_i)_{SAA}$, $(h_i)_{SAA}$ is the prior PSF information and known.) by using the following error-metric,

$$E_{SAA} = \left\|h_{SAA} - \hat{h}_{SAA}\right\|^2 \tag{12}$$

The algorithm minimizes on the combined error metrics described above, with weights, i.e.

$$E = \alpha_1 E_F + \alpha_2 E_{BL} + \alpha_3 E_{SAA} \tag{13}$$

where α_1, α_2 and α_3 are weights.

4. ERROR METRIC MINIMIZATION

The proposed algorithm follows a conjugate gradient technique[7, 8] for error metric minimization. To apply conjugate gradient minimization efficiently, it is necessary to calculate the derivatives of error metric.

Next, we demonstrate the derivatives of errors[2]. Assume that

$$L = \sum_k \left\|G_k'\right\|^2 - \left\|\frac{\sum_k G_k'^* \hat{H}_k}{\left(\gamma + \sum_k \left|\hat{H}\right|^2\right)^{\frac{1}{2}}}\right\|^2 \tag{14}$$

The partial derivatives of L can be taken as

$$\frac{\partial L}{\partial \hat{h}_j(n)} = -\sum_u \frac{\partial}{\partial \hat{h}}\left(\frac{\left|\sum_k G_k'^*(u)\hat{H}_k(u)\right|^2}{\gamma + \sum_k \left|\hat{H}_k(u)\right|^2}\right)$$

$$= -\sum_u \frac{\left(\sum_k G_k'^* \partial\hat{H}_k \sum_k G_k' \hat{H}_k^* + \text{c.c.}\right)\left(\gamma + \sum_k \left|\hat{H}_k\right|^2\right) - \left|\sum_k G_k'^* \hat{H}_k\right|^2 \left(\sum_k \hat{H}_k^* \partial\hat{H}_k + \text{c.c.}\right)}{\left(\gamma + \sum_k \left|\hat{H}_k\right|^2\right)^2}$$

$$= -\sum_u \frac{\left(\gamma + \sum_k \left|\hat{H}_k\right|^2\right) \sum_k G_k' \hat{H}_k^* \sum_k G_k'^* \partial\hat{H}_k - \left|\sum_k G_k'^* \hat{H}_k\right|^2 \sum_k \hat{H}_k^* \partial\hat{H}_k}{\left(\gamma + \sum_k \left|\hat{H}_k\right|^2\right)^2} + \text{c.c.}$$

$$= -\sum_u \sum_k Z_k \partial\hat{H}_k + \text{c.c.} = -\sum_u Z_j(u)\,\partial\hat{H}_j(u) + \text{c.c.} = -\sum_u Z_j(u)\exp(-i2\pi < u, n > /N) + \text{c.c.}$$

$$= -\text{FFT}\left[Z_j\right](n) + \text{c.c.} \tag{15}$$

where the u dependence has been suppressed; the summation over k runs from 1 to K; the prime applied to a function signifies a partial derivative; c.c. represents a term that is the complex conjugate of the preceding term; and we have defined

$$\mathrm{Z_k(u)} = \frac{\mathrm{G}_k^{\prime *}\left(\gamma + \sum_k\left|\widehat{\mathrm{H}}_k\right|^2\right) \quad \sum_k \mathrm{G}_k^{\prime}\widehat{\mathrm{H}}_k^* - \left|\sum_k \mathrm{G}_k^{\prime *}\widehat{\mathrm{H}}_k\right|^2\widehat{\mathrm{H}}_k^*}{\left(\gamma + \sum_k\left|\widehat{\mathrm{H}}_k\right|^2\right)^2} = \frac{\mathrm{G}_k^{\prime *}\left(\gamma + \sum_k\left|\widehat{\mathrm{H}}_k\right|^2\right) \quad \sum_k \mathrm{G}_k^{\prime}\widehat{\mathrm{H}}_k^* - \left|\sum_k \mathrm{G}_k^{\prime}\widehat{\mathrm{H}}_k^*\right|^2\widehat{\mathrm{H}}_k^*}{\left(\gamma + \sum_k\left|\widehat{\mathrm{H}}_k\right|^2\right)^2} \tag{16}$$

On the other hand, [2]the partial derivatives of the discrete Fourier transforms of PSFs corresponding to the PSFs can be computed as

$$\frac{\partial \widehat{\mathrm{H}}_k(\mathrm{u})}{\partial \widehat{\mathrm{h}}_j(\mathrm{n})} = \begin{cases} \exp(-\mathrm{i}2\pi < u, n > /N) & \mathrm{k = j} \\ 0 & \mathrm{k \neq j} \end{cases} \tag{17}$$

where n and u are the spatial index and the spatial frequency index respectively, and $< u, n >$ denotes the inner product. The partial derivatives of $\mathrm{E_{BL}}$ can be represented as

$$\frac{\partial \mathrm{E_{BL}}}{\partial \widehat{\mathrm{h}}_j(\mathrm{n})} = \sum_u \sum_k \Lambda \widehat{\mathrm{H}}_k^* \, \partial \widehat{\mathrm{H}}_k + \mathrm{c.c.} = \mathrm{FFT}\left(\Lambda \widehat{\mathrm{H}}_j^*\right) + \mathrm{c.c.} \tag{18}$$

5. NUMERICAL SIMULATIONS

In this section we present the results for single star and binary star from noisy-free case to Gaussian noise case, in order to illustrate the reliability and practicality of algorithm on AO data. In addition, numerical simulation of Phase Screen[9, 10, 11, 12] distorted by atmospheric turbulence following the Kolmogorov spectrum by using Fourier Transform is also done to make PSFs, so that the low-order corrected astronomical images are gotten by convolution of ideal-star images and PSFs, and Gaussian noise. Here, the sizes of all images are 64×64 pixels. We assume that $\mathrm{f_c} = 23$ pixels and $\mathrm{D/r_0} = 10$, where D is the diameter of a telescope and $\mathrm{r_0}$ is the Fried parameter. Finally, one thousand short exposure PSFs are averaged to get one long exposure PSF. The simulations use 5 diffraction limited PSFs (Fig.1 shows one frame) and 45 PSFs distorted by atmospheric turbulence (Fig.1 shows 6 frames). The ideal images of single star and binary stars are respectively gotten by sampling a 2-D gauss function and a function gotten by adding 2 2-D gauss functions (Fig.2 shows ideal images). In this section, the degraded images are achieved by convolution of ideal-star images and PSFs, and Gaussian noise.

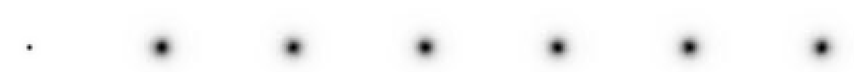

Fig.1: Left to right, diffraction limited PSF and six PSFs distorted by atmospheric turbulence.

Fig.2: Left to right, ideal single-star image and ideal binary-star image

5.1 The numerical simulation of single-star restoration

Simulations are applied to single-star degraded images in which Gaussian noise with three cases (0 means and 0, 0.001, 0.01 standard deviations) is added. In our simulations the effectivity of constraint represented by formulation (12) are not marked, so the numerical simulations don't use it. The simulations use two basic formulations presented here.

$$E = \alpha_1 E_F + \alpha_2 E_{BL} \tag{19}$$

where α_1 and α_2 are weights. And,

$$E_F = \sum_k \left\| G'_k \right\|^2 - \left\| \frac{\sum_k G'^{*}_k \hat{H}_k}{\left(\gamma + \sum_k \left|\hat{H}_k\right|^2\right)^{\frac{1}{2}}} \right\|^2 \tag{20}$$

5.1.1 Simulation 1 (for noisy-free images)

The initial inputs of simulation are 8 degraded images and 2 initial estimates of PSF showed in Fig.3. The outputs of simulation are the optimal estimates of ideal single-star image. Finally, these estimates are fitted by Gaussian functions. Fig.4 and Fig.5 show these results. Initial parameters and performance of algorithm are shown in Table 1. The central position and FWHM (full width at half maximum) of star by fitting optimal estimate of ideal single-star image are shown in Table 2. From Table 2 the star in results image is sharper than one in degraded image, and we can even get diffraction-limited image.

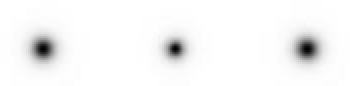

Fig.3: Left to right, degraded image (here only one frame), ideal PSF and single-star image used as initial estimates of PSF

Fig.4: Left to right, for ideal PSFs inputs the first four images are the restorations for 2, 4, 6 and 8 frames. The last four images are the Gaussian-fitting results for the first four images, respectively.

Fig.5: Left to right, for single-star PSFs inputs the first four images are the restorations for 2, 4, 6 and 8 frames. The last four images are the Gaussian-fitting results for the first four images, respectively.

Table1: The parameters and performance of algorithm.

PSF	frame	γ	α_1	α_2	E	iteration	Time (second)
ideal	2	500000	1.0	0.005	-2.18343e+010	5	27.169
	4	500000	1.0	0.005	-4.40983e+010	4	40.718
	6	500000	1.0	0.005	-6.61401e+010	3	49.982
	8	500000	1.0	0.005	-8.87499e+010	3	78.362
Single-star	2	1e+006	1.0	0.001	-2.18895e+010	6	31.676
	4	1e+006	1.0	0.001	-4.4181e+010	7	61.138
	6	1e+006	1.0	0.001	-6.62492e+010	7	100.084
	8	1e+006	1.0	0.001	-8.88867e+010	7	147.311

Table2: Gaussian-fitting results

		Central position (pixel)	FWHM (pixel)
Ideal image		(17.0000,17.0000)	4.7079
Diffraction-limited image		(17.0018, 16.9913)	5.3253
Degraded image		(17.0108, 16.9877)	8.7855
Ideal PSFs	2 frame	(16.9375, 17.0682)	5.5125
	4 frame	(16.9404, 17.0467)	5.2121
	6 frame	(16.9602, 17.0298)	5.0601
	8 frame	(16.9693, 17.0403)	5.0263
Single-star PSFs	2 frame	(16.9403, 17.0650)	5.7231
	4 frame	(16.9378, 17.0369)	5.4825
	6 frame	(16.9640, 17.0197)	5.2891
	8 frame	(16.9740, 17.0300)	5.1864

5.1.2 Simulation 2 (Gaussian noise)

Simulation 2 has two processes (represented by P1 and P2) that are all same as simulation 1. P1 is used for the degraded images in which Gaussian noise with zero mean and 0.001 standard deviation is added. Initial inputs of P1 is shown in Fig.6 consisted of the degraded image , the ideal PSF and the single-star image that is used as initial estimates of PSFs and that is added in by Gaussian noise with zero mean and 0.001 standard deviation. Fig.7 and Fig.8 show the results of restoration and Gaussian fitting for this case. The central position and FWHM gotten by fitting optimal estimates of ideal single-star image are shown in Table 3.

P2 is used for the degraded images in which Gaussian noise with zero mean and 0.01 standard deviation is added. Initial inputs of P2 is shown in Fig.9 consisted of the degraded image , the ideal PSF and the single-star image that is used as initial estimates of PSFs and that is added in by Gaussian noise with zero mean and 0.01 standard deviation. Fig.10 and Fig.11 show the results of restoration and Gaussian fitting for this case. The central position and FWHM gotten by fitting optimal estimates of ideal single-star image are shown in Table 4.

From Table 3 and Table 4 choosing better initial estimates of PFS, the algorithm can improve the sharpness of star.

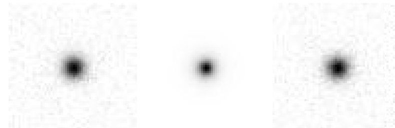

Fig.6: Left to right, degraded image (here only one frame), ideal PSF and single-star image used as initial estimates of PSFs

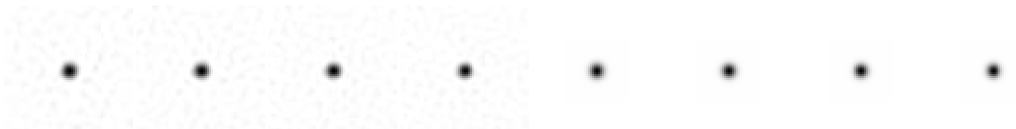

Fig.7: Left to right, for ideal PSFs inputs the first four images are the restorations for 2, 4, 6 and 8 frames. The last four images are the Gaussian-fitting results for the first four images, respectively.

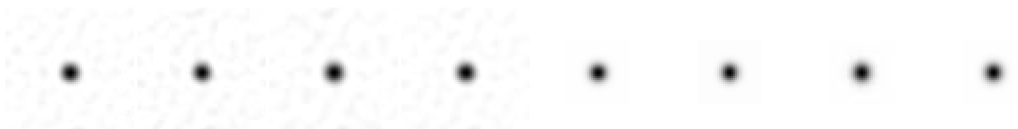

Fig.8: Left to right, for single-star PSFs inputs the first four images are the restorations for 2, 4, 6 and 8 frames. The last four images are the Gaussian-fitting results for the first four images, respectively.

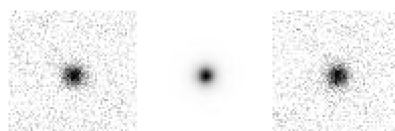

Fig.9: Left to right, degraded image (here only one frame), ideal PSF and single-star image used as initial estimates of PSFs

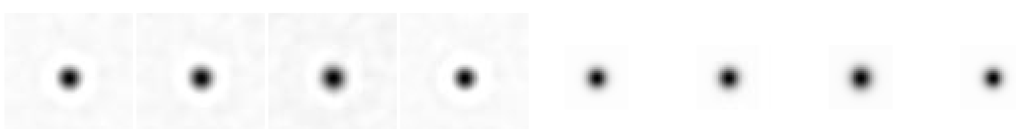

Fig.10: Left to right, for ideal PSFs inputs the first four images are the restorations for 2, 4, 6 and 8 frames. The last four images are the Gaussian-fitting results for the first four images, respectively.

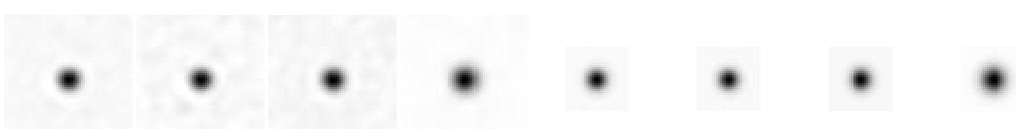

Fig.11: Left to right, for single-star PSFs inputs the first four images are the restorations for 2, 4, 6 and 8 frames. The last four images are the Gaussian-fitting results for the first four images, respectively.

Table 3: Gaussian-fitting results

		Central position (pixel)	FWHM (pixel)
Ideal image		(17.0000,17.0000)	4.7079
Diffraction-limited image		(17.0018, 16.9913)	5.3253
Degraded image		(16.9784, 16.9570)	8.7863
Ideal PSFs	2 frame	(16.9667, 17.1096c	5.4137
	4 frame	(17.0201, 17.0695)	5.3960
	6 frame	(17.0613, 17.0632)	5.2421
	8 frame	(17.0888, 17.0563)	5.1682
Single-star PSFs	2 frame	(16.8761, 17.0009)	6.5708
	4 frame	(16.7734, 16.9075)	6.6266
	6 frame	(16.8677, 16.9406)	7.2022
	8 frame	(16.7596, 16.8984)	6.8531

Table 4: Gaussian-fitting results

		Central position (pixel)	FWHM (pixel)
Ideal image		(17.0000,17.0000)	4.7079
Diffraction-limited image		(17.0018, 16.9913)	5.3253
Degraded image		(16.9339, 17.0117)	8.2798
Ideal PSFs	2 frame	(16.9511, 16.9859)	8.6320
	4 frame	(16.9330, 16.9680)	7.9697
	6 frame	(16.9298, 17.0046)	7.6176
	8 frame	(16.9429, 17.0024)	7.3877
Single-star PSFs	2 frame	(16.9476, 16.8558)	8.3581
	4 frame	(16.9196, 16.8167)	7.8574
	6 frame	(16.9274, 16.8577)	8.0128
	8 frame	(16.9934, 16.8640)	9.9721

5.1.3 Conclusion

1) Using better initial estimates of PSFs, the algorithm can better restore the position of single star and maintain the shape of single star.
2) The Gaussian fitting can better correct the distortion of star shape and can suppress some noise.
3) When the Gaussian noise is bigger, the algorithm can't effectively restore the single star. For example, in the case that the Gaussian noise with zero mean and 0.1 standard deviation is added to the degraded images, the noise almost submerges stars and the numerical simulation also show that the stars can't be restored.

5.2 The numerical simulation of binary-star restoration

Simulations are applied to binary-star degraded images in which Gaussian noise with two cases (0 means and 0, 0.01 standard deviations) is added. The simulations use the model formulations (19) and (20).

5.2.1 Simulation 1 (for noisy-free images)

The initial inputs of simulation are 8 degraded images and 3 initial estimates of PSF showed in Fig.12. The outputs of simulation are the optimal estimates of ideal binary-star image. Finally, these estimates are fitted by 2 2-D Gaussian functions. Fig.13, Fig.14 and Fig.15 show these results. The central position and FWHM gotten by fitting initial estimates of PSFs and fitting optimal estimates of ideal binary-star image are shown in Table 5 and Table 6 respectively. From Table 6 the algorithm can improve the resolution and contrast of binary star.

Fig.12: Left to right, the degraded image (here only one frame), the ideal PSF and the single-star-1 and single-star-2 images used as initial estimates of PSFs

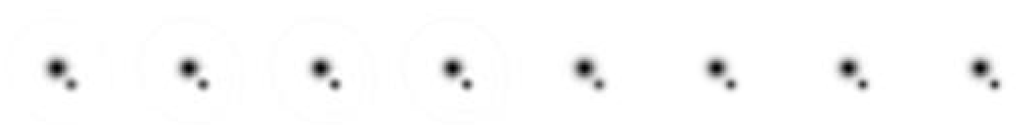

Fig.13: Left to right, for ideal PSFs inputs the first four images are the restorations for 2, 4, 6 and 8 frames. The last four images are the Gaussian-fitting results for the first four images, respectively.

Fig.14: Left to right, for single-star-1 PSFs inputs the first four images are the restorations for 2, 4, 6 and 8 frames. The last four images are the Gaussian-fitting results for the first four images, respectively.

Fig.15: Left to right, for single-star-2 PSFs inputs the first four images are the restorations for 2, 4, 6 and 8 frames. The last four images are the Gaussian-fitting results for the first four images, respectively.

Table 5: Gaussian fitting of PSFs

PSF	Central position (pixel)	FWHM (pixel)
Ideal	(17.0577, 16.9397)	7.1740
Single-star-1	(17.0452, 16.9341)	8.2749
binary-star-2	(17.0286, 16.9764)	8.8188

Table 6: Gaussian-fitting results

		Central position 1 (pixel)	FWHM 1 (pixel)	Central position 2 (pixel)	FWHM 2 (pixel)	Relative distance (pixel)
Binary-star image		(14.0005, 14.0004)	7.0647	(21.0012, 22.0007)	3.5334	10.63
Diffraction-limited image		(14.0027, 14.0069)	7.6091	(20.9898, 21.9937)	4.2268	10.61
Degraded image		(14.1044, 14.0576)	10.6151	(21.1292, 22.1126)	8.0338	10.69
Ideal PSFs	2 frame	(13.9486, 14.0645)	7.4312	(20.9339, 22.0293)	4.7528	10.59
	4 frame	(13.9408, 14.0239)	7.1119	(20.8912, 21.9958)	4.4294	10.58
	6 frame	(13.9259, 14.0372)	7.0614	(20.8779, 21.9913)	4.3003	10.56
	8 frame	(13.9342, 14.0338)	7.0522	(20.8691, 21.9892)	4.2361	10.55
Single-star-1 PSFs	2 frame	(13.9552, 14.0791)	7.8697	(20.9571, 22.0410)	4.9699	10.60
	4 frame	(13.9343, 14.0267)	7.5068	(20.9261, 22.0162)	4.6377	10.62
	6 frame	(13.9142, 14.0274)	7.2895	(20.9145, 22.0204)	4.4481	10.63
	8 frame	(13.9123, 14.0225)	7.1254	(20.9096, 22.0195)	4.3315	10.63
Single-star-2 PSFs	2 frame	(16.9726, 17.0737)	7.8655	(24.0620, 25.1585)	4.6880	10.75
	4 frame	(17.0408, 17.1348)	7.9319	(24.0170, 25.1104)	4.4779	10.60
	6 frame	(17.0498, 17.1770)	7.9813	(23.9900, 25.0935)	4.3478	10.53
	8 frame	(17.0614, 17.1820)	7.9702	(23.9833, 25.0827)	4.2672	10.50

5.2.2 Simulation 2 (Gaussian noise)

The process of simulation 2 is same as simulation 1. The degraded images possess of Gaussian noise with zero mean 0.001 standard deviation. Fig. 16 is consisted of the degraded image , the ideal PSF and the binary-star image that is used as initial estimates of PSFs and that is added by Gaussian noise with zero mean and 0.001 standard deviation. Fig. 17 and Fig. 18 show the results of restoration and Gaussian fitting. The central position and FWHM gotten by fitting optimal estimates of ideal binary-star image are shown in Table 7. From Table 7 the algorithm can improve the resolution and contrast of binary star.

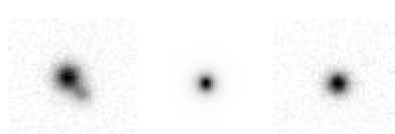

Fig.16: Left to right, degraded image (here only one frame), ideal PSF and single-star image used as initial estimates of PSFs

Fig.17: Left to right, for ideal PSFs inputs the first four images are the restorations for 2, 4, 6 and 8 frames. The last four images are the Gaussian-fitting results for the first four images, respectively.

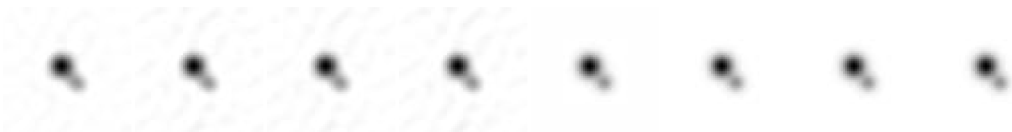

Fig.18: Left to right, for single-star PSFs inputs the first four images are the restorations for 2, 4, 6 and 8 frames. The last four images are the Gaussian-fitting results for the first four images, respectively.

Table 7: Gaussian-fitting results

		Central position 1 (pixel)	FWHM 1 (pixel)	Central position 2 (pixel)	FWHM 2 (pixel)	Relative distance (pixel)
Binary-star image		(14.0005, 14.0004)	7.0647	(21.0012, 22.0007)	3.5334	10.63
Diffraction-limited image		(14.0027, 14.0069)	7.6091	(20.9898, 21.9937)	4.2268	10.61
Degraded image		(14.0171, 14.0385)	10.4625	(21.1213, 22.0533)	8.1519	10.71
Ideal PSFs	2 frame	(13.9092, 13.9591)	7.7495	(21.0582, 21.8765)	6.0084	10.67
	4 frame	(13.9303, 13.9129)	7.4512	(21.0258, 21.8977)	5.5880	10.67
	6 frame	(13.9707, 13.9031)	7.2438	(21.0142, 21.9345)	5.2615	10.68
	8 frame	(13.9842, 13.9098)	7.1772	(21.0004, 21.9348)	4.9432	10.66
Single-star PSFs	2 frame	(13.8783, 13.9507)	8.5929	(21.0244, 22.0120)	6.8935	10.77
	4 frame	(13.8992, 13.8763)	8.5284	(20.8441, 22.0201)	6.7490	10.70
	6 frame	(13.9180, 13.8798)	8.6452	(20.8668, 22.0205)	6.8314	10.70
	8 frame	(13.9303, 13.8807)	8.6093	(20.8668, 22.0567)	6.7134	10.72

5.2.3 Conclusion

1) Using better initial estimates of PSFs, the algorithm can keep the relative distance of binary stars and the bigger star. When the initial estimates of PSFs are not ideal, the algorithm effect declines.
2) The Gaussian fitting can better correct the distortion of star shape.
3) When the Gaussian noise is bigger, the algorithm can't effectively restore the binary star.

6. SUMMARY

The variability and the lack of a precise frame-by-frame PSF determination make post-processing of the data difficult. The multi-frame iterative deconvolution method described takes successfully advantage of this variability. Numerical simulation of Phase Screen distorted by atmospheric turbulence following the Kolmogorov spectrum by using Fourier Transform is made in this paper to generate the PSFs which are used to simulate the degraded images through atmospheric turbulence. The multi-frame iterative deconvolution is used to process these images. It can reduce the turbulent effect and improves the resolution and contrast of stars.

7. References:

[1]Li Qiang, SHEN Mang-zuo, “The study of high-resolution imaging of astronomical object based on phase-diversity method”. Chinese Astronomy and Astrophysics，2007.48(1):113-120.

[2]Jefferies, S.M. & Christou, J.C., “Restoration of astronomical images by iterative blind deconvolution”, Astrophys. J. , 1993, 415, 862.

[3] Julian C. Christou, E. Keith Hege , Stuart M. Jefferies , & Christoph U. Keller,” Application of Multi-frame Iterative Blind Deconvolution for Diverse Astronomical Imaging”, SPIE Vol. 2200, 433-444.

[4] Julian C. Christou,” Blind Deconvolution Post-processing of Images Corrected by Adaptive Optics”, SPIE Vol. 2534, 226-234.

[5] Julian C. Christou, Domenico Bonaccini, Nancy Ageorges,” Deconvolution of Adaptive Optics Near-Infrared System (ADONIS) Images”, SPIE Vol. 3126 ,78.

[6] J.C. CHRISTOU, D. BONACCINI, N. AGEORGES, and F. MARCHIS,” Myopic Deconvolution of Adaptive Optics Images”, ESO, no.97-sep99/messenger-no.97,14-22.

[7]William H.Press, Saul A.Teukolsky, William T.Vetterling, Brian P.Flannery, “Numerical Recipes in C++ ”, the art of scientific computing, second edition, BeiJing: Publishing house of electronics industry.

[8]Jorge Nocedal, Stephen J.Wright, “Numerical Optimization”, www.sciencep.com.

[9]Benjamin L. McGlamery, ” Computer simulation studies of compensation of turbulence degraded images”, SPIE/OSA, Vol.74 (1976) Image Processing, 225-233.

[10] E.M.Johansson, D.T.Gavel, ”Simulation of stellar speckle imaging”, SPIE,1994,2200:372-383.

[11] M.C.Roggemann, B.M.Welsh, ”Imaging through turbulence”, New York: CRC Press,1995.

[12] Lijing Wang, LI Qiang, WEI Hong-gang , LIAO Sheng , SHEN Mang-zuo ,“Numerical simulation and validation of phase screen distorted by atmospheric turbulence”, Opto-Electronic Engineering, 2007, 34(3): 1-4.